

BEAM HALO IN PROTON LINAC BEAMS

T.P.Wangler, Los Alamos National Laboratory, Los Alamos, NM 87545

K.R.Crandall, TechSource, Santa Fe, NM 87594-1057

Abstract

We review the present understanding of beam halo in proton linacs. Space-charge forces acting in mismatched beams have been identified as a major cause of beam-halo. We introduce a new description of the halo using the ratio of moments of the distribution of beam coordinates. We describe the beam-halo experiment that is in preparation at Los Alamos, which will address questions about the beam profiles, maximum particle amplitudes, and rms-emittance growth associated with the halo.

1 INTRODUCTION

The existence of beam halo is an important characteristic of high-intensity beams. Under certain conditions a small fraction of particles can acquire enough transverse energy from the repulsive space-charge forces within the beam to form a halo. Halo formation is an important concern because halo particles in proton linacs can be lost on the walls of the beamline structures, where they will induce unwanted radioactivity. New high-power proton-linac applications, including accelerators to produce tritium¹, and to transmute radioactive wastes², are affected by the increased risk of beam loss from halo.

One may wonder why beams develop halo. Halos observed in computer simulations can form as a consequence of classical filamentation in 6D phase space from nonlinear space-charge forces. The 6D phase-space filaments project as an extended diffuse halo into the 2D spaces where they are observed.³ But one should recognise that halo in real beams may include additional sources that are not yet included in the simulation codes.

2 DESCRIPTION OF HALO

There is no clearly defined separation between the halo and the main core of the beam. Consequently, there has been some difficulty identifying a suitable quantitative measure of the halo content of a beam in a model-independent way. A general characteristic of beam halo is the increased population of the outer part of the beam. To describe this feature in coordinate space, we introduce a new quantity, which we call the beam-profile parameter. For a continuous beam we define the beam-profile parameter for the transverse x-coordinate as

$$h_x = \langle x^4 \rangle / \langle x^2 \rangle^2 - 2,$$

and a similar definition can be made of h_y , by replacing y for x . For an ellipsoidal beam bunch the definition for the x-coordinate is

$$h_x = \langle x^4 \rangle / \langle x^2 \rangle^2 - 15/7,$$

and likewise for h_y and h_z in the other two directions. These are dimensionless parameters, which are independent of the beam intensity, easily calculated from measured or simulated particle distributions, dependent only on the profile shapes, and zero for a uniform-density beam, which has no halo. As halo develops in the beam, increasing the relative population of particles with large transverse amplitudes, the beam-profile parameters increase. We have evaluated the beam-profile parameters for some familiar 2D and 3D distributions in Table 1.

Table 1: Some beam-profile parameter values.

Spatial Distribution	Beam-profile parameter h_x
Uniform ellipse (K-V)	0
Parabolic (4D Waterbag)	1/4
Gaussian ellipse	1
Uniform ellipsoid	0
Parabolic ellipsoid	4/21
Gaussian ellipsoid	6/7

Using this description, we can consider some interesting physics questions related to the shape of the beam profile, such as, whether there a relationship between rms-emittance growth and growth of the beam-profile parameter. Using computer simulations we have examined several common cases. We find that rms-matched beams that evolve in linear focusing channels and beams that expand in free space can have beam-profile parameters that decrease, even though the rms emittance grows. Thus, when the charges redistribute to provide the proper Debye shielding within the beam and field energy is converted to thermal energy⁴, emittance growth occurs without growth of the beam-profile parameter. The beam density becomes more uniform, and the emittance growth is associated with an increased spread in momentum space, a temperature increase. For rms-mismatched beams halo growth is correlated with increases in the beam-profile parameter and the rms emittance. This suggests that rms emittance can increase without halo growth, but halo growth always leads to emittance growth.

Simulations suggest that halo becomes a significant feature of the density distribution when the beam-profile

parameter exceeds values near 1, the value for a Gaussian beam. We adopt the beam-profile parameter of the Gaussian distribution, which is near to or equal to unity as an approximate threshold for significant halo content. With this criterion, the familiar equilibrium beams and rms-matched beams used in computer simulations lie below halo threshold. Even a Gaussian beam is very compact; although theoretically Gaussian beams extend to infinity, their density falls off very rapidly and by our criterion lie just at the halo threshold. Rms-mismatched beams can develop very extended halos with large beam-profile parameters in the range of 5 to 10.

It is useful to introduce an equivalent Gaussian beam (same rms size and total current as the real beam) as a reference distribution. We can estimate the percentage of particles in the halo from the percentage of particles with displacements beyond some standard displacement that are in excess of the equivalent Gaussian distribution. An attractive choice for a standard displacement is 2.2σ , which is based on consideration of the family of halo-free beam distributions that are uniform in N dimensions, requiring that none of these can contribute to the percentage of halo particles. The resulting halo percentage for rms-mismatched beams in simulations is a few percent.

The halo description above still does not fully characterize the halo. Another important quantity of practical interest is the maximum amplitude of the halo particles. For comparison of simulations with predictions of the particle-core model discussed in the next section, it has been convenient to calculate, using high statistics runs, the dimensionless ratio of the maximum amplitude of a mismatched beam to the rms size of a matched beam.

When exciting a pure mode in a FODO channel, the initial mismatch strength for each coordinate x , y , and z can be measured by a mismatch parameter μ . For each coordinate the value of μ relates the mismatched Courant-Snyder parameters α and β at the symmetry point midway between quadrupoles to the matched parameters α_m and β_m , given as $\alpha = \mu^2 \alpha_m$ and $\beta = \mu^2 \beta_m$. For a matched beam $\mu = 1$, and for real linacs effective values of μ in the approximate range 0.7 to 1.3 might be expected as a result of random parameters errors. Different modes can be excited by the proper relative choices of μ for the different coordinates. For simulation of a pure breathing-mode mismatch at the location midway between the quadrupoles, one can choose $\mu_x = \mu_y$.

3 BEAM HALO IN PROTON LINACS

The subject of beam halo has been reviewed recently⁵ where the reader will find many published references. In numerical simulation studies of space-charge dominated rms-mismatched beams,⁶ an outer halo is observed in the particle distributions that is much more extended and more densely populated than the small Debye tail at the edge of a matched beam. The simulation results suggest a particle-core model to describe the motion of halo

particles in a mismatched beam.⁷ In the model the radius of a central charge distribution or core oscillates as a consequence of a mismatch. Individual beam particles are represented by test particles that interact with the external focusing force and with the time-dependent space-charge field of the core. An important result obtained from an approximate analytic solution of the model equations⁸ has been the discovery that the interaction between the particles and the oscillating core is described by a parametric resonance that is effective in driving some particles to large amplitudes. The parametric resonance affects particles whose oscillation frequencies are about one half the frequency of the oscillating core. This simple model is sufficient to describe approximately the maximum amplitudes that are observed in the beam-dynamics simulations in uniform-focusing channels.

In a typical proton linac, bunches are formed which have an approximately ellipsoidal shape in the beam frame with a range of aspect ratios that may include very long bunches to nearly spherical bunches. To model the transverse dynamics of halo particles in mismatched beams, where the bunch length is several times larger than the radius, it is convenient to use a simple particle-core model based on transverse particle motion in the space-charge field of a radially oscillating cylindrical beam core. To model the halo-particle dynamics for a spherical bunch one can use a particle-core model with a spherical core. The space-charge field of the beam is approximated by replacing the beam distribution with that of an equivalent-uniform beam core, where the equivalent core has the same rms size as the actual beam. Except for a KV distribution or a matched beam in the extreme space-charge limit, the test particles that are most strongly driven by the resonance mostly represent the particles that populate a finite size Debye tail at the edge of the real beam. The fraction of those particles that are included within the region of influence of the resonance determines approximately the population of the halo. We have found that the particle-core model results are not sensitive to choice of the core-density distribution.

We find from simulations that the maximum amplitude for any mismatch strength is proportional to the matched rms beam size. Using the analytic solution relating the matched rms size of the beam core to the current, emittance, and focusing strength, we have obtained a scaling formula for the size of the transverse beam halo.⁵ The formula predicts that for a given mismatch strength the maximum transverse halo amplitude increases with increasing beam current, and with decreasing frequency, bunch length, and focusing strength. Estimates of the growth time of the halo have been made from numerical studies of the model. Generally, these growth times are not very sensitive to the mismatch strength, but increase strongly with tune-depression ratio as the beam becomes more emittance dominated. The halo growth times from the simulations depend on the initial particle distribution, and are often difficult to define in an unambiguous way.

As the beam becomes more space-charge dominated, chaotic motion is observed. The chaos does not substantially increase the maximum amplitude, but may increase the population of the halo.

The simple spherical model is a first approximation for a bunched beam with nearly equal semi-axes excited in a breathing mode. But the spherical model neglects several effects, two other core-oscillation modes (quadrupole mode and antisymmetric mode), effects associated with aspect ratios different than unity, and nonlinear rf longitudinal external fields. The study of a more general ellipsoidal bunch model^{9,10} shows that the halo physics depends on the bunch-aspect ratio. For long bunches (approximately $z > 2r$) the transverse and longitudinal envelope and halo dynamics are weakly coupled. The breathing mode is dominated by transverse motion and generates transverse halo. The antisymmetric mode where the longitudinal core oscillations are out of phase with the transverse core oscillations is dominated by longitudinal motion and generates longitudinal halo. For nearly spherical bunches the transverse and longitudinal envelope and halo dynamics are strongly coupled.

Nonlinear rf focusing has been added to the particle-core model¹¹ to represent the nonlinear rf effects in the longitudinal dynamics. As the longitudinal particle amplitudes increase, a defocusing nonlinear longitudinal force term adds significantly to the main linear term to impede the increase in the net focusing force and disrupt the parametric-resonance condition. The model and the simulations show that the longitudinal halo is well confined within the rf bucket except for extreme values of the mismatch. Beam loss from longitudinal halo may be less of a concern in a linac than the transverse halo.

4 BEAM HALO EXPERIMENT

We are installing a beamline at the end of the Low-Energy Demonstration Accelerator (LEDA)¹² to carry out the first experimental study of beam-halo formation in a proton beam (see Fig.1). A 6.7-MeV, 100-mA proton beam from the 350-MHz radio-frequency quadrupole (RFQ)¹³ will be injected into the new beamline. The beamline consists of a 10.9-m FODO array of 52 quadrupole magnetic lenses for transverse confinement of the beam, and beam-diagnostic devices to monitor and measure the beam properties. To study the beam halo we will set the first four quadrupole strengths to establish matching or different mismatching conditions more or less favorable for halo formation, and measure and analyse the beam profiles. The measured halo effects will be compared with those predicted by our beam-dynamics simulation codes, and the comparisons will enable us either to confirm that the computer simulations are correct or identify possible missing physics effects that may need to be incorporated. We will measure the maximum excursions of the beam, and the particle distributions including the corresponding beam-profile parameters. We

will also calculate the rms emittances of the beam, which can be obtained from the rms sizes by measuring beam profiles at different locations. An important experimental objective is to explore those regions beyond where halo is predicted by the simulation codes to investigate other possible sources of halo.

The detailed theoretical predictions of the beam halo are made using beam-dynamics codes based on multiparticle simulation methods to follow the evolution of the beam particles. Included are the quadrupole focusing forces and the repulsive space-charge forces that act on all the particles. The simulation codes all contain certain approximations, and different computer codes are used to provide internal checks.

The experiment uses the output beam from the LEDA RFQ. The beam leaves the RFQ as a sequence of subnanosecond bunches at a 350-MHz rate. To avoid beam destruction of the thin wires used for measurement of the beam profiles, the beam will be pulsed at about a 1- to 2-Hz rate with short 20- to 30-microsecond long macropulses. As the beam propagates along the beamline, the bunches expand longitudinally and eventually after a few meters each bunch overlaps with adjacent bunches forming an approximately continuous beam. The main effect of the debunching is to reduce the effective beam current and accompanying space-charge forces that affect the transverse halo formation. The transverse tune-depression ratio from space-charge ranges from 0.7 to 0.9. The magnitude of the halo for mismatched beams with $\mu=2$ is predicted to be large and easily measurable.

The mismatch-induced beam oscillations in a continuous beam consist of two kinds, a breathing mode, where the oscillations in the two transverse planes x are in phase, and a quadrupole mode, where the oscillations are out of phase.

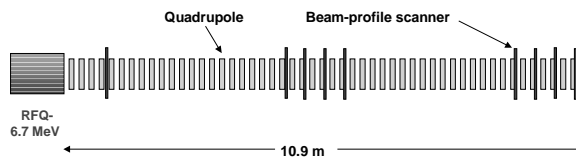


Fig.1. Block diagram of beam-halo experiment showing the 52-quadrupole lattice and locations of the beam-profile scanners.

The transverse beam profiles will be measured using an array of specially constructed beam-profile scanners.^{14,15} The scanners are located nominally at the middle of some of the drift spaces between pairs of quadrupoles. Each scanner contains a single 33-micron diameter graphite wire for measurements of the high-intensity central beam core in each transverse plane. In addition each scanner contains a pair of copper plates, one on each side of each wire to intercept and measure the beam intensity in the low-density halo region. The beam-profile scanner provides intensity measurements over a dynamic range of

about 10^6 . For a beam with a Gaussian profile, the device provides a transverse profile measurement out to more than 5σ . This sensitivity will be suitable for detecting the halo predicted by the simulations as well as to search for other possible halo sources. Other aspects of the experiment are described by papers at the conference.^{16,17}

5 SIMULATION STUDIES

Figures 2 through 5 show some beam-dynamics simulation results for the breathing-mode mismatched beam with $\mu=2$, using 10,000 particles per simulation run and using the SCHEFF¹⁸ space-charge subroutine. Figs. 2, 3, and 5 show results at the centers of the 52 drift spaces along the beamline. The input-particle distribution for the simulations was obtained from a previous beam-dynamics simulation through the LEDA RFQ. Fig. 2 shows the rms beam sizes in x and y and the maximum particle displacements. The in-phase oscillations for x_{rms} and y_{rms} indicate that the breathing-mode has been excited. There is a large factor of about 2 increase in the maximum particle amplitude compared with the matched beam (not shown). Fig. 3 shows the beam-profile parameter for both matched and mismatched cases for the y coordinate versus distance along the beamline. The values for uniform (KV), parabolic (4D Waterbag), and Gaussian beams are shown for reference. The oscillations at the breathing-mode frequency are the result of the rotation of the outer phase-space filaments that constitute the halo as they alternately project into either coordinate space, where it shows up in the beam-profile parameter, or momentum space, where it does not. The excursions above the Gaussian level indicate growth of a large beam halo. Fig. 4 shows the beam cross section at the center of drift space after quadrupole 49 showing the halo. Fig. 5 shows rms-emittance growth in the x and y planes versus distance along the beamline. Breathing-mode simulations with 100M particles, using a 3D space-charge code IMPACT¹⁹ on a fast parallel computer agree well with the results shown in the figures. The maximum amplitudes from the 100M particle simulation are larger than those of the SCHEFF runs by only about 10%. Rms emittances and beam-profile parameters for the two codes agree to within about 10%. Nevertheless, the simulation results will depend on the actual input beam distribution which may differ from that assumed in these initial simulations.

6 SUMMARY

We have reviewed the present understanding of beam halo in proton linacs. Beam mismatch acts in two ways to produce the halo. First, even without space-charge forces, a mismatch produces coherent oscillations of the beam particles and an immediate increase in particle transverse amplitudes. Second, the nonlinear space-charge force, acting while the beam particles are oscillating through the beam, slowly drives some particles to larger amplitudes

through parametric resonance and increases the beam profile parameter.

We have presented a new description of halo based on the moments of the distribution of particle coordinates. We have introduced the Gaussian distribution as a reference for determining when a significant halo is present and for estimating the fraction of beam in the halo. We have described the beam-halo experiment in preparation at the LEDA facility at Los Alamos, which will provide the first experimental tests of our understanding of halo formation in high-current proton beams. Experimental measurements are expected from October through the early part of 2001.

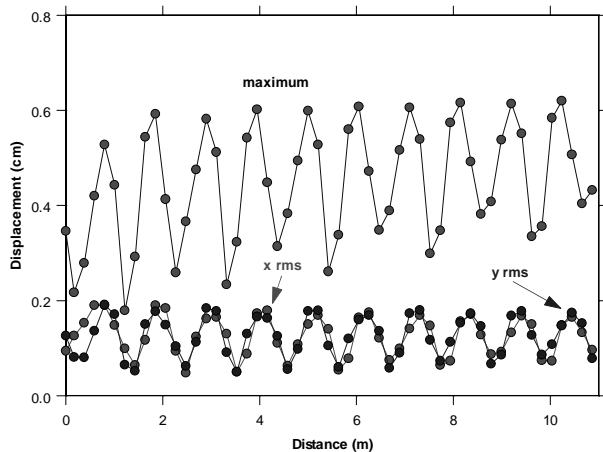


Fig. 2. Rms beam sizes and maximum particle displacements from computer simulation at the 52 drift-space locations along the beamline for the breathing-mode mismatched beam with $\mu=2$.

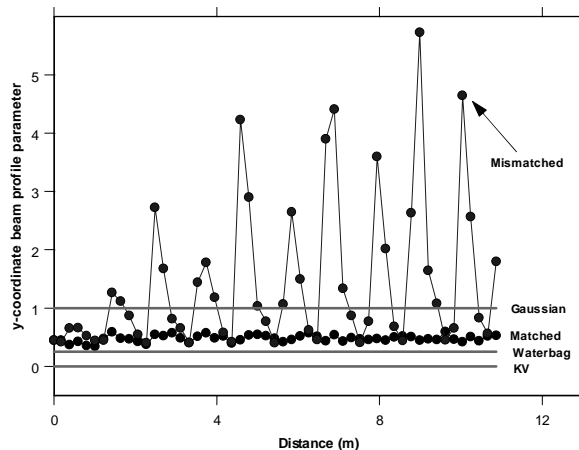


Fig. 3. Beam-profile parameter in the y coordinate from computer simulation at the 52 drift-space locations along the beamline for the matched and breathing-mode mismatched beam with $\mu=2$. Values for uniform (KV), parabolic (4D Waterbag), and Gaussian beams are shown for reference. The excursions above the Gaussian level indicate a large halo.

ACKNOWLEDGMENTS

The authors acknowledge support from the U.S. Department of Energy, and thank R.L.Gluckstern, A. Jason, R.D.Ryne, J.D.Gilpatrick, and C.K.Allen for valuable discussions. We thank Ji Qiang for the simulations he carried out using the 3D IMPACT code.

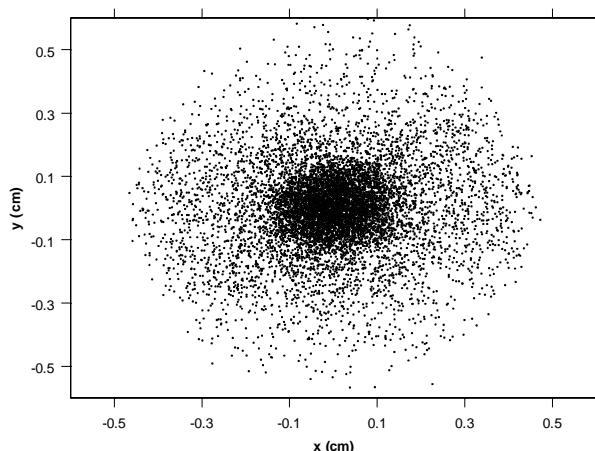


Fig. 4. Beam cross section from computer simulation showing the presence of halo at center of the drift space after the quadrupole 49 for the breathing-mode mismatched beam with $\mu=2$.

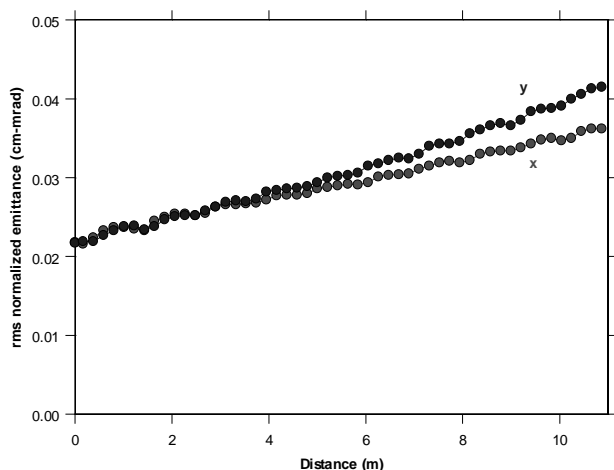


Fig. 5. Rms emittances in x and y planes for breathing-mode mismatched beam with $\mu=2$ at the 52 drift-space locations along the beamline.

REFERENCES

- ¹ P.W.Lisowski, "The Accelerator Production of Tritium Project," Proc. 1997 Particle Accelerator Conf., Vancouver, British Columbia, Canada, (IEEE, Catalog No.97CB36167, 1997) 3780-3784.
- ² "A Roadmap for Developing Accelerator Transmutation of Waste (ATW) Technology," A Report to Congress, DOE/RW-0519, October 1999.

- ³ T. P. Wangler, Computational Accelerator Physics Conference (CAP93), 1993, AIP Conf. Proc. **297**, edited by Robert Ryne, (AIP Press, New York, 1993), p 9.
- ⁴ T. P. Wangler, K. R. Crandall, R. S. Mills, and M. Reiser, IEEE Trans. Nucl. Sci. **32**, 2196 (1985).
- ⁵ Thomas P. Wangler, "Beam Halo Formation in High Intensity Proton Beams", Proc. 2nd ICFA Advanced Accelerator Workshop on the Physics of High Brightness Beams, November 9-12, 1999, UCLA, Los Angeles, CA.
- ⁶ A. Cucchetti, M. Reiser, and T. P. Wangler, Proceedings of the IEEE 1991 Particle Accelerator Conference, 1991, IEEE Catalog No. 91CH3038-7, edited by L. Lizama and J. Chew, (IEEE, New York, 1991), p. 251.
- ⁷ For an introduction see T. P. Wangler, K. R. Crandall, R. Ryne, and T. S. Wang, Phys. Rev. ST Accel. Beams **1**, (084201) 1998.
- ⁸ R. Gluckstern, Phys. Rev. Lett. **73**, 1247 (1994).
- ⁹ R. L. Gluckstern, A. V. Fedotov, S. S. Kurennoy, and R. D. Ryne, Phys. Rev. E. **58**, 4977 (1998).
- ¹⁰ Ji Qiang and Robert D. Ryne, "Beam halo studies using three dimensional particle-core model," Phys.Rev. ST Accel.Beams **3**, 064201(2000).
- ¹¹ J. Barnard and S. Lund, 1997 Particle Accelerator Conf., Vancouver, British Columbia, Canada, p. 1929 and p.1932.
- ¹² J.D.Schneider, "Operation of the Low-Energy Demonstration Accelerator: The Proton Injector for APT,"Proc. 1999 IEEE Particle Accelerator Conf. (IEEE Catalog No.CH36366, 1999), pp.503-507.
- ¹³ D. Schrage et al., "CW RFQ Fabrication and Engineering," Proc. XIX International Linac Conference (Argonne National Laboratory, ANL-98/28, 1998), 679-683.
- ¹⁴ J. D. Gilpatrick, D. Barr, D. Bruhn, L. Day, J. Ledford, M. Pieck, R. Shurter, M Stettler, R. Valdiviez, J. Kamperschroer, D. Martinez, J. O'Hara, M. Gruchalla, and D. Madsen, "Beam Diagnostics Instrumentation for a 6.7-MeV Proton Beam Halo Experiment," these proceedings.
- ¹⁵ R. Valdiviez, N. Patterson, J. Ledford, D. Bruhn, R. LaFave, F. Martinez, A. Rendon, H. Haagenstad, J. D. Gilpatrick, and J. O'Hara, "Intense Proton Core and Halo Beam Profile Measurement: Beam Line Component Mechanical Design," these proceedings.
- ¹⁶ P.L.Colestock, et al., "The Beam Halo Experiment at the LEDA Facility," these proceedings.
- ¹⁷ L.Day et al, "Control System for the LEDA 6.7 MeV Proton Beam Halo Experiment," these proceedings.
- ¹⁸ Thomas P. Wangler, "Principles of RF Linear Accelerators" (John Wiley & Sons, 1998), pp 270-272.
- ¹⁹ J. Qiang, R. D. Ryne, S. Habib, V. Decyk, "An Object-Oriented Parallel Particle-in-Cell Code for Beam Dynamics Simulation in Linear Accelerator," J. Comput. Phys. **163**, 1 (2000).